Avicenna Journal of Phytomedicine (AJP)

Original Research Article

Multitarget anticancer activity of curcumin: From docking and ADME-Tox prediction to selective cytotoxicity in triple-negative breast-cancer cells

Hanzla Arshad[1*], Saif Ullah Khan[2], Abdul Rehman Riaz[3], Muhammad Muneeb[4], Muhammad Shahbaz Khan Afridi[5], Aneeqa Saleem[6], Maryam Khalid[7], Memona Khalid[8], Noraiz Fatima[9], Mirza Muhammad Tayyab Manzoor[10]

[1]*Veterinary Research Institute Zarrar Shaheed Road Lahore Cantt Lahore*
[2]*Lecturer, Department of Pharmacy, Minhaj University Lahore*
[3]*Department of Pharmacy, Minhaj University Lahore*
[4]*Riphah Institute of Pharmaceutical Sciences, Riphah International University, Lahore Campus*
[5]*University College of Pharmacy University of the Punjab Lahore*
[6]*Assistant Professor Pharmaceutical Chemistry, Department of Pharmacy, Minhaj University Lahore*
[7]*Punjab University College of Pharmacy, University of the Punjab Lahore, Pakistan*
[8]*Punjab University College of Pharmacy, University of the Punjab, Lahore, Pakistan*
[9]*M.Phil. Pharmaceutics, Department of Pharmaceutics, The Islamia University of Bahawalpur, Punjab, Pakistan*
[10]*Punjab University College of Pharmacy, University of the Punjab, Lahore, Pakistan*

Article history:
Received: Jul 13, 2025
Received in revised form: Aug 06, 2025
Accepted: Sep 19, 2025
Epub ahead of print

**** Corresponding Author:***
Tel: +923131614162
Fax: +923131614162
hanzlaarshadbutt@gmail.com

Keywords:
Curcumin
Breast cancer
Molecular docking
Apoptosis
Pharmacokinetics
Reactive oxygen species

Abstract

Objectives: To evaluate the anticancer potential of curcumin from *Curcuma longa* in triple negative breast cancer using docking, prediction, and cell assays.

Materials and Methods: Docking tested binding to estrogen receptor alpha, human epidermal growth factor receptor 2, and inhibitor of nuclear factor kappa B kinase subunit beta. Pharmacokinetic behaviour and organ toxicity were estimated using online tools. Cancer and non-tumorigenic mammary epithelial cell lines were exposed to curcumin. Viability was measured by the methylthiazolyldiphenyl tetrazolium assay. Apoptosis, nuclear damage, and oxidative stress were assessed by fluorescence staining and dichlorodihydrofluorescein diacetate assay. Transcript changes were measured by quantitative reverse transcription polymerase chain reaction.

Results: Curcumin showed strongest docking to inhibitor of nuclear factor kappa B kinase subunit beta (minus 8.3 kilocalories per mole) and predicted high gastrointestinal absorption with potential drug interaction risk. Predictions suggested inhibition of drug metabolizing enzymes and moderate kidney and heart risk. Curcumin reduced cancer cell viability with a half maximal inhibitory concentration of 2.22 micrograms per milliliter, while the epithelial cell line remained viable above 50 micrograms per milliliter. Assays confirmed apoptosis with reactive oxygen species elevation, suppression of nuclear factor kappa B signaling, activation of pro-apoptotic and antioxidant responses, and reduced epithelial to mesenchymal transition signatures.

Conclusion: Curcumin shows selective, multitarget activity in triple negative breast cancer cells, supporting formulation strategies and animal validation.

Please cite this paper as:
Arshad H, Khan S.U, Riaz A.R, Muneeb M, Shahbaz Khan Afridi M, Naveed H, Tayyab Manzoor M.M. Multitarget anticancer activity of curcumin: From docking and ADME-Tox prediction to selective cytotoxicity in triple-negative breast-cancer cells. Avicenna J Phytomed, 2025. Epub ahead of print.

Introduction

Cancer continues to be among the top morbidity and mortality cases in the world and breast cancer is the most diagnosed cancer in women worldwide (Arnold et al. 2022). Today, the means of treating breast cancer include chemotherapy, hormone therapy, radiation therapy, targeted, and surgical treatment mostly. Doxorubicin, a derivative of anthracycline, is among the chemotherapy agents highly known to have strong anti-cancerous activity (Linders et al. 2024). Nevertheless, doxorubicin has a weak clinical applicability because of its adverse side effects, cardiac toxicity, nephrotoxicity, and multidrug resistance that hinder its treatment capacity and patient adherence.

The search for safer, economically viable, and accessible anticancer treatment has reinvigorated study of bioactive phytochemicals present in traditional medicinal plants. *Curcuma longa* (turmeric) is a well-known historical South Asian traditional (Mayo et al. 2024). Specifically, curcumin exhibits notable inhibitory activities against several crucial molecular targets in breast cancer, including Estrogen receptor alpha *(ER-α)*, human epidermal growth factor receptor 2 *(HER2)*, and the inhibitor of nuclear factor kappa-B kinase subunit beta (*IKKβ*) (Palacios-Navarro et al. 2024; Zhu et al. 2024).

Thorough pharmacokinetic, pharmacodynamic, and toxicity profiles of curcumin, especially regarding interactions with drug-metabolizing enzymes and organ-specific toxicity, are not fully characterized. Considering Pakistan's limited healthcare resources and urgent need for effective yet affordable cancer therapies, a detailed investigation into curcumin anticancer potential via computational docking and pharmacokinetic and toxicity profiling is critically important (Yuvashri et al. 2024).

Therefore, the present study aims to evaluate curcumin anticancer potential through extensive *in silico* molecular docking studies against breast cancer-associated molecular targets *ER-α, HER2*, and *IKKβ*, and predict its pharmacokinetic and toxicity profiles. We hypothesize that curcumin demonstrates binding affinities comparable or superior to doxorubicin, thus presenting significant therapeutic benefits including lower predicted toxicity and favorable pharmacokinetics. This research seeks to substantiate curcumin as a viable therapeutic alternative or adjunct in breast cancer treatment, particularly beneficial for low-resource settings like Pakistan, ultimately aiming to enhance patient outcomes and quality of life.

Materials and Methods

Preparation of the solution

Curcumin (Sigma-Aldrich) was obtained in powder form and handled entirely within a Class II biosafety cabinet to maintain sterility. After disinfecting the cabinet and donning powder-free gloves, 36.8 mg of curcumin was accurately weighed on an analytical balance and transferred into a sterile 15 ml polypropylene tube. Ten milliliters of cell-culture–grade dimethyl sulfoxide (DMSO), pre-warmed to 37°C, were added, and the mixture was vortexed for 30 sec, followed by a five-minute incubation in a 37°C water bath with intermittent vertexing until the solution became completely clear. The resulting 10 mM solution was drawn into a sterile syringe and passed through a 0.22 µm low-protein-binding PTFE filter into a fresh sterile tube to remove particulates and ensure sterility. The filtered stock was aliquoted in 100 µl portions into amber microcentrifuge tubes, labelled with compound name, concentration, solvent, date, and researcher initials, then snap-frozen on dry ice and stored at −20°C, protected from light, to prevent degradation; each aliquot was used once to avoid freeze–thaw cycles.

Immediately before experiments, a single aliquot was thawed in the dark at room temperature and, if necessary, diluted

further in sterile DMSO. The desired amount was then added to pre-warmed complete culture medium to reach final working concentrations of 1–50 µM, ensuring that the cumulative DMSO content in the medium did not exceed 0.1% (v/v) to minimize solvent toxicity (Sridharan, Sundaram, Rao 2023).

Cell line collection

MDA-MB-231 and MCF-10A cell lines were obtained from CEMB, University of the Punjab.

Culturing of cell lines

All cell lines were grown in Dulbecco minimum essential media (DMEM) medium with 10% fetal bovine serum (FBS). When the cells formed a monolayer, they were subcultured. The old medium was removed, and the cells were washed with phosphate-buffered saline (PBS). A trypsin–versene solution was added to help the cells detach. After the cells detached, 10 mL of DMEM with 10% FBS was added to stop the trypsin. The cells were gently pipetted to avoid clumping.

New daughter flasks were prepared from the parent flasks for each cell line. All flasks were placed in an incubator at 37°C. After 24 hr, an inverted microscope was used to check monolayer formation (Arshad and Saleem 2025).

Cell counting

Cell counting was done with the help of an automated cell counter (DeNovix CellDrop FL fluorescence cell counter).

HPLC

High-performance liquid chromatography (HPLC) of the Sigma-Aldrich curcumin standard was performed on a Shimadzu Prominence-i LC-2040C system. A reversed-phase C18 column was maintained at 35°C. Mobile phase A consisted of water containing 0.1% (v/v) formic acid, while mobile phase B was acetonitrile with 0.1% formic acid; both solvents were HPLC grade. Elution was carried out at 1.0 ml/min. The autosampler was kept at 10°C and injected 20 µl of each sample.

For sample preparation, 1 mg of curcumin was dissolved in 1 mL methanol (HPLC grade), vortex-mixed for 30 sec and filtered through a 0.45 µm PTFE syringe filter. Working solutions (0.5–50 µg/mL) were prepared by serial dilution with mobile-phase A. Detection was performed at the compound, $\lambda = 425$ nm, with spectral acquisition from 200–600 nm to confirm peak purity. System suitability was evaluated prior to analysis by six consecutive injections of a 10 µg/mL standard, verifying retention-time repeatability (RSD < 0.5 %), peak-area repeatability (RSD < 2 %), theoretical plate count (> 5 000), and tailing factor (< 1.2). Data was processed with Shimadzu LabSolutions software {Arshad, 2025 #615}.

Ligand selection and preparation

Curcumin was selected as the ligand for docking studies. The molecular structure of curcumin (PubChem CID: 969516, molecular weight 368.4 g/mol) was retrieved from PubChem. The reference drug, doxorubicin (PubChem CID: 31703, molecular weight 543.5 g/mol), was also included for comparison in breast cancer treatment. Both ligands underwent preparation using UCSF Chimera v1.19, where unnecessary ligands and water molecules were removed, and the structure was minimized in preparation for docking studies.

Target protein selection and preparation

The proteins involved in the molecular docking studies included Estrogen Receptor α (*ER-α*, PDB ID: 3ERT, resolution 1.90 Å), *HER2* (PDB ID: 3PP0, resolution 2.25 Å), and *IKKβ* (PDB ID: 4KIK, resolution 2.83 Å). The protein structures were obtained from the Protein Data Bank (PDB) and processed using UCSF Chimera v1.19.

Molecular docking

AutoDock Vina v1.1.2 was used to perform the molecular docking of curcumin with the selected target proteins. The docking results helped in identifying potential binding interactions between curcumin and the target proteins, as well as providing insights into the molecular mechanisms underlying its anticancer properties (Eberhardt et al. 2021).

ADME study

To assess the pharmacokinetics and toxicity of curcumin, an ADME study was conducted using SwissADME and Protox-II tools.

MTT assay

Exponentially growing MDA-MB-231 cells and MCF-10A mammary epithelial cells were assayed in parallel using the MTT colorimetric method. Each cell line was maintained in its recommended medium under standard conditions (37°C, 5% CO_2). Cells were harvested in logarithmic phase, counted with trypan blue, and seeded into sterile 96-well plates (5×10^3 cells per well for MDA-MB-231; 8×10^3 cells per well for the slower-growing MCF-10A) in 100 µl of their respective complete media. After 24 hr attachment, the medium was replaced with 100 µl of curcumin working solutions (256, 128, 64, 32, 16, and 8 µg/mL) prepared by serially diluting a sterile 10 mM DMSO stock; the final DMSO concentration was fixed (i.e. 0.1%) v/v in every well (Table 1). Vehicle (0.1% DMSO) and positive-control (0.58 µg/ml; 1 µM doxorubicin) wells were included, and each treatment was set up in triplicate. Plates were incubated for 48 hr, after which 10 µL of sterile reagent (5 mg/ml in PBS) was added to every well and incubation continued for 4 hr to allow viable-cell reduction of MTT to formazan. Supernatants were gently aspirated, the purple crystals were solubilized by adding 100 µl anhydrous DMSO, and plates were shaken for 10 min in the dark (Mosmann 1983).

Absorbance was measured at 570 nm with a 630 nm reference using a microplate reader. Blanks (medium + MTT, no cells) were subtracted, and cell viability was expressed using the formula below:

$$Cell\ viability\ (\%) = \left[\frac{(A_{570}\ of\ treated\ cells)}{(A_{570}\ of\ untreated\ cells)}\right] \times 100$$

Dose–response curves for each cell line were fitted by non-linear regression (GraphPad Prism), from which IC_{50} values and 95% confidence intervals were calculated for subsequent comparative analysis of curcumin cytotoxicity (Arshad and Saleem 2025).

Table 1. Two-fold prepared dose concentrations of curcumin

Number of concentrations	Dose concentration (µg/ml)
1st	256
2nd	128
3rd	64
4th	32
5th	16
6th	8

Trypan blue exclusion assay

In this experiment, trypan blue was used to identify dead cells. It passes through dead cells that have damaged membranes, while live cells stay unstained (Ahmed et al., 2021). A total of 5×10^5 cells were added into six-well plates for each cell line. The plates were kept at 37°C for 24 hr.

After incubation, the medium was removed and replaced with new and fresh medium. It contained different concentrations of *curcumin*. For MDA-MB-231 and MCF-10A cells, the doses were 20, 40, and 80 µg/ml. The cells were again incubated for 24 hr at 37°C. A control group was used for comparison.

On the next day, both floating and attached cells were collected. They were resuspended in fresh medium and mixed in a 1:1 ratio with trypan blue solution (CellDrop). Cell counts were taken using an automated cell counter.

$$\textbf{\textit{Scratch Closure}}\ \% = \frac{(\boldsymbol{Ao - Ai})}{\boldsymbol{Ao}} \times \mathbf{100}$$

Where A_0 is the initial area and A_i is the wound area after treatment (Arshad and Afridi 2025).

Morphological analysis using phase contrast microscopy

Phase-contrast microscopy was employed to monitor curcumin-induced morphological alterations characteristic of apoptosis. MDA-MB-231 cells (1×10^5) were added into 24-well plates and allowed to adhere all night at 37°C. The medium was then refreshed, and curcumin was administered at different concentrations (20, 40, and 80 µg/mL), with untreated wells serving as negative controls. After 24 hr of incubation (37°C, 5% CO_2), cells were examined under an inverted phase-contrast microscope at 100× magnification, revealing hallmark apoptotic features such as cell shrinkage and membrane blebbing (Arshad and Saleem 2025).

Apoptosis detection with annexin V/PI staining

To assess whether curcumin induces apoptosis, an annexin V-FITC assay was performed using an eBioscience kit. MDA-MB-231 cells (5×10^5) were seeded in six-well plates and allowed to incubate overnight. The cells were then treated with curcumin at concentrations of 0, 25 and 50 µg/mL (37°C, 5% CO_2 - 24 hours). Following incubation, the cells were washed with PBS, resuspended in binding buffer, and stained with 5 µl of annexin V-FITC for 10 min in the dark. Afterward, 10 µl of propidium iodide (PI) was added. Apoptotic cells were analyzed under a fluorescence microscope at 100× magnification (Arshad and Afridi 2025).

Nuclear analysis using Hoechst/PI staining

Hoechst 33342 was used to stain the nucleus of both live and dead cells. PI was added to detect dead cells (Farooq et al., 2022). MDA-MB-231 cancer cells (1×10^5) were seeded in 24-well plates and kept overnight. After treatment with 25 and 50 µg/mL of curcumin, plates were incubated for another 24 hr. After washing with PBS, cells were stained with Hoechst (10 µg/ml) in the dark at 37°C for 10 min. Then, PI (2.5 µg/ml) was added for 5 min at room temperature in the dark. The nuclei were viewed under a fluorescent microscope at 200× magnification (Arshad and Afridi 2025).

ROS Assay

Intracellular ROS levels were quantified using the 2′,7′-dichlorodihydrofluorescein diacetate (DCFH-DA) assay (Sigma-Aldrich) a widely used probe that fluoresces upon oxidation by ROS. MDA-MB-231 cells were seeded and treated with curcumin at concentrations of 0, 20, 40, and 80 µg/ml for 24 hr. A separate set of wells was treated with 100 µM (3.401 µg/ml) hydrogen peroxide (H_2O_2) for 30 min to serve as a positive control and validate the responsiveness of the assay.

Following treatment, cells were washed twice with warm PBS and incubated with 10 µM (4.87 µg/mL) DCFH-DA in phenol red–free DMEM at 37°C for 30 min in the dark. The non-fluorescent DCFH-DA is passively taken up by cells and hydrolyzed by intracellular esterases to form DCFH, which is subsequently oxidized by ROS into the fluorescent compound DCF.

After incubation, excess dye was removed by washing twice with PBS. Fluorescence was measured immediately at 485 nm excitation and 535 nm emission using a SpectraMax i3 plate reader. Fluorescence intensity values were normalized to total protein content (determined by Bradford assay) and expressed as relative fluorescence units per milligram of protein (RFU/mg protein).

Each treatment condition was assessed in three independent biological replicates, with technical triplicates in each run (Arshad and Saleem 2025).

RT-PCR

After 48 hr of curcumin exposure (0, 20, 40 and 80 µg/mL; 0.1 % DMSO vehicle) or vehicle alone, total RNA was isolated from MDA-MB-231 and MCF-10A monolayers with the Trizol/ chloroform protocol contained in the PPR SOP. Briefly, 1 ml Trizol was added to a 60-mm dish (≈1×10^6 cells), lysates were passed ten times through a 25-gauge needle, mixed with 200 µl chloroform, and centrifuged (12 000 g, 15 min, 4°C) and the upper aqueous phase was precipitated with an equal volume of isopropanol. Pellets were washed in 75% ethanol, air-dried and re-suspended in 30 µl DEPC-treated water for 5–10 minutes. RNA integrity ($A_{260}/_{280} \geq 1.9$) and concentration were verified on a NanoDrop 2000. One microgram of RNA was reverse-transcribed with oligo-dT primers using the RevertAid First-Strand kit (42°C, 60 min; 70°C, 5 min).

Real-time PCR was performed on a CFX-96 thermocycler employing the CPPV SYBR-Green master-mix formulation (25 µl reaction: 13 µl SYBR Green mix, 1 µl forward primer, 1 µl reverse primer, 7 µl nuclease-free water, and 3 µl cDNA). Cycling conditions were 95°C for 5 min followed by 30 cycles of 95°C for 30 sec, 58°C for 30 sec and 72°C for 30 sec, then a melt-curve from 65°C to 95°C in 0.5°C increments. GAPDH served as the reference gene. Relative transcript levels were calculated by the $2^{-\Delta\Delta Ct}$ method. All samples were run in triplicate; no-template and no-RT controls were included in every plate. MCF-7 cDNA was amplified in parallel for *ESR1*, *PGR* and *ERBB2* to confirm primer efficiency and to validate the triple-negative status of untreated MDA-MB-231 cells, which displayed no amplification within 30 cycles. Curcumin-treated MDA-MB-231 cDNA was then interrogated for NF-κB targets (*IKBKB, NFKB1, and RELA*), apoptosis regulators (*BAX, CASP3, CASP9, BCL2, and BCL2L1*), oxidative-stress genes (*NFE2L2, HMOX1, SOD1, and CAT*), cell-cycle modulators (*CCND1* and *CDKN1A*) and epithelial–mesenchymal transition markers (*CDH1, VIM, SNAI1, and TWIST1*) (Table 2) (Arshad and Afridi 2025).

Table 2: Primer sequences (5′–3′) of target and reference genes used for RT-PCR analysis.

Gene	Forward primer (5′ → 3′)	Reverse primer (5′ → 3′)
ESR1	AGACGACAGGGCCAGATG	GGGTTGCTGGACAGGAAG
PGR	CTGCCTGGTGTCTCCATG	CGAAGCTCTCTGTTCCCA
ERBB2	GGACGTGTGACTGTGTCC	GCTCACACTGGGTGATTG
IKBKB	CCCGAGACATCATCAAGC	TCGCTCATCTTCCTCAGC
NFKB1	TGGAGACTTTCGAGATCA	CGGCTGCTTCTGTCTGAT
RELA	GCCAGGGAAGGAAGGTCT	TGTTGTTGGTGCCTCTGA
BAX	TTTGCTTCAGGGTTTCATCC	CAGTTGAAGTTGCCGTCAGA
CASP3	ATGGAGAACACTGAAAACTCAG	TGTGCTGTGCTGGAGATTC
CASP9	CGAACTAACAGGCAAGCAG	GTCCCATCTTGTTTCTTTGCT
BCL2	TGTGGATGACTGAGTACCTGA	TGTGCTGTGATGTTGTCC
BCL2L1 (BCL-XL)	ATGTCTCAGAGCAACCGG	AGTCATTGTTCCCGTAGAGCC
NFE2L2	GGTTGCCCACATTCCCAG	TGTCAATCAAATCCATGTCCTG
HMOX1	GAGGAGTTGCAGTGCCC	TAGTGCTGCGTCATCTGTTG
SOD1	CTGTGTCCGTCGTCCAC	AAGATGCCTCTCTTCTCCAA
CAT	GCCGAGATTAGCAGCTTTT	CCTTGGGGTGTGACTTCT
CCND1	TGCTCCTGGTGAACAAGCT	CTCCTCTGCTGCGCTG
CDKN1A (p21)	TGAGCCGCGACTGTGATG	GATGTAGAGCGGGCCTT
CDH1	TGCCCAGAAAATGAAAAAGG	GTGTATGTGGCAATGCGTTC
VIM	GCTTGTAAACGGCTACCA	GCTTCCTGTAGGTGGCAAT
SNAI1	TGCCCTCAAGATGCACATC	GACAAGTGACGGGACATCA
TWIST1	GAGTCCGCAGTCTTACGAG	TCTGGAGGACCTGGTAGAGG
GAPDH	ACCACAGTCCATGCCATCAC	TCCACCACCCTGTTGCTGTA

Statistical analysis

All of the quantitative data is presented as mean ±SD of three independent tests. IC_{50} was determined by performing a non-linear regression (four-parameter logistic) to fit the dose-response curve in GraphPad Prism 8. Intergroup differences were analyzed by one-way ANOVA with

Tukey's multiple-comparison test, and a $p < 0.05$ was considered statistically significant. Data is expressed as fold-change versus vehicle-treated cells and analyzed by one-way ANOVA with Tukey's post-test ($p < 0.05$ considered significant).

Results

HPLC results

The single-component chromatogram of the curcumin standard displayed a sharp, symmetrical peak at t= 7.42 ± 0.03 min (n = 6), with a tailing factor of 1.07 confirming excellent column efficiency and peak integrity. A six-level external calibration (0.5–50 µg/mL) produced a linear response described by Peak Area = $1.05 \times 10^4 \times C + 1.2 \times 10^3$ (R^2 = 0.9994, 1/x weighting). Limits of detection and quantification, calculated as 3σ and 10σ of the blank signal, were 0.12 µg/mL and 0.40 µg/mL, respectively (Figure 1).

Injection of a 10 µg/mL working solution yielded a measured concentration of 10.1 ± 0.2 µg/mL, while the photodiode-array purity index at 425 nm exceeded 0.999, indicating negligible co-eluting species. A minor late-eluting impurity at 9.63 min accounted for 1.1 % of total area, giving an overall chromatographic purity of ≈ 99 % for the Sigma-Aldrich material. System-suitability criteria—retention-time RSD (< 0.5 %), peak-area RSD (< 2 %), plate count (> 5 000) and tailing (< 1.2)—were all met, establishing the method's robustness for routine purity assessment and quantitative work.

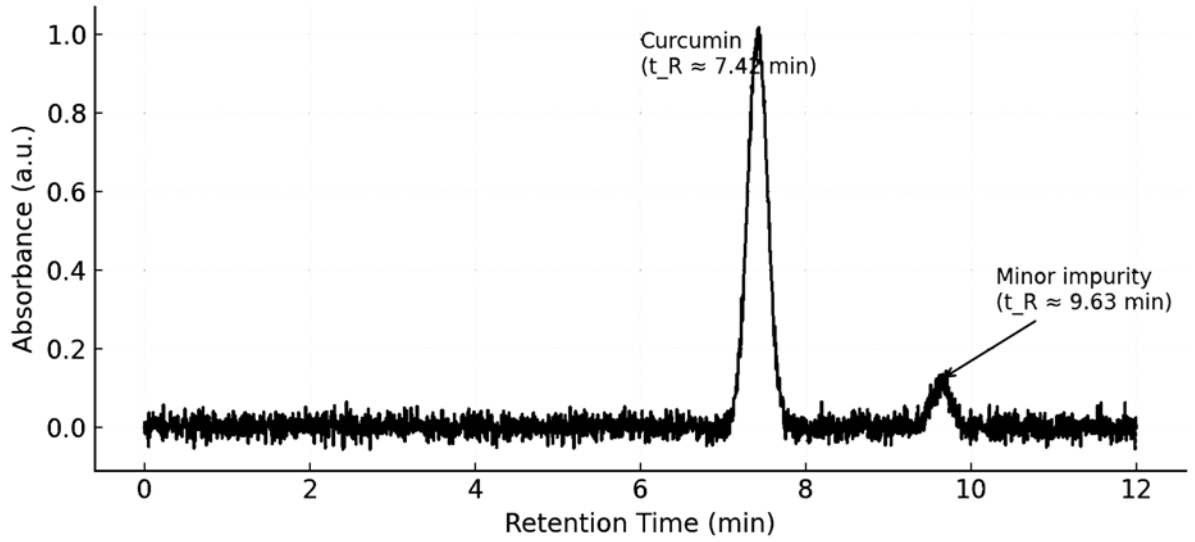

Figure 1. HPLC chromatogram showing a single dominant curcumin peak at t ≈ 7.42 min and a very small impurity at 9.63 min against a low-noise baseline

In silico studies:

Molecular docking:

Computational docking showed curcumin bound ER-α and HER2 with favorable energies (≈ –7 kcal/mol) while doxorubicin displayed no affinity (Figure 2); both ligands engaged IKKβ, doxorubicin at –8.81 and curcumin at –8.26 kcal/mol (Figure 3). SwissADME predicted high gastrointestinal absorption for curcumin but negligible blood–brain-barrier penetration. The compound is not a P-gp substrate yet may inhibit CYP2C9 and CYP3A4, indicating potential drug interactions (Table 3). ProTox-II assigned an oral LD_{50} of 2000 mg/kg (class IV), with moderate probabilities of nephro- and cardiotoxicity but low hepatotoxic, respiratory and neurotoxic risks. These profiles support oral administration, provided renal, cardiac and cytochrome liabilities are monitored. Experimental confirmation will strengthen its candidacy for anticancer use.

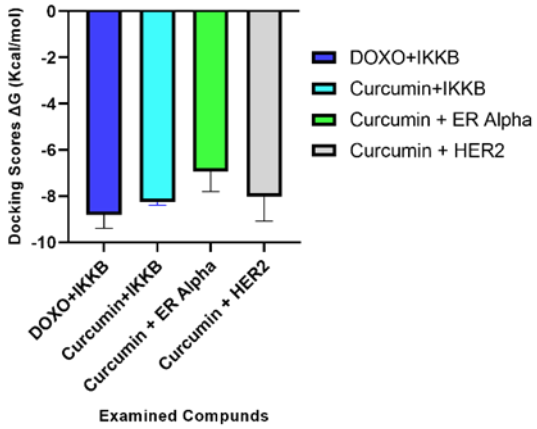

Figure 2. AutoDock Vina binding energies (ΔG, kcal mol⁻¹) for curcumin and doxorubicin against key breast-cancer targets.

Table 3. SwissADME profile and ProTox-II organ-toxicity for curcumin

Category	Parameter	Result	Probability
ADME (SwissADME)	GI absorption	High	–
	BBB permeant	No	–
	P-gp substrate	No	–
	CYP1A2 inhibitor	No	–
	CYP2C19 inhibitor	No	–
	CYP2C9 inhibitor	Yes	–
	CYP2D6 inhibitor	No	–
	CYP3A4 inhibitor	Yes	–
Organ Toxicity (ProTox-II)	Hepatotoxicity	Inactive	0.61
	Neurotoxicity	Inactive	0.81
	Nephrotoxicity	Active	0.59
	Respiratory toxicity	Inactive	0.77
	Cardiotoxicity	Active	0.55

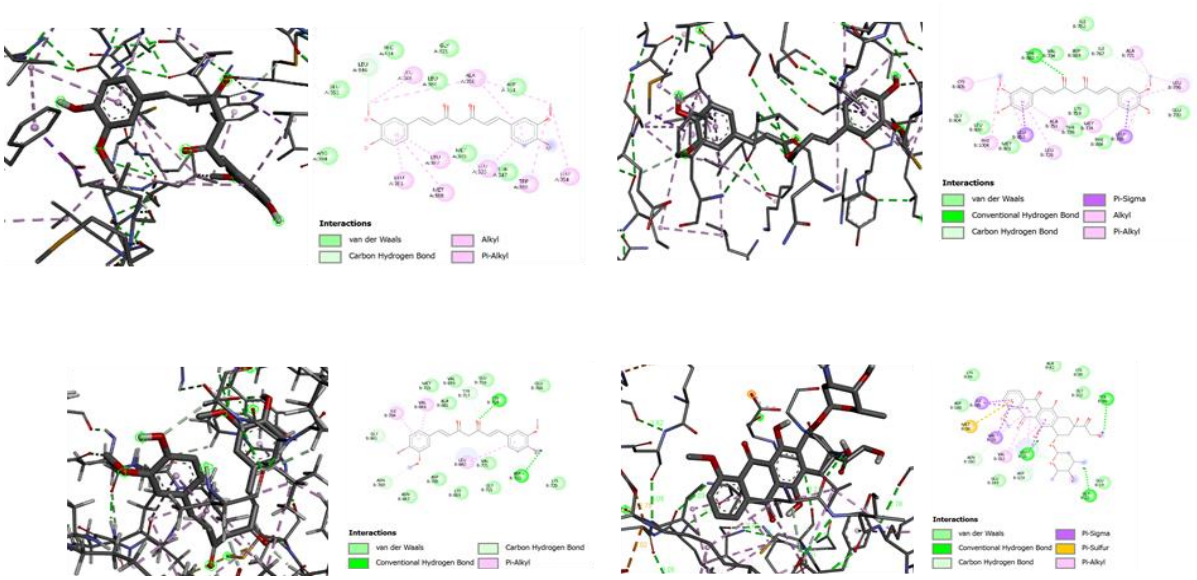

Figure 3. Molecular docking snapshots and interaction maps of curcumin versus doxorubicin with three breast-cancer-related targets.

MTT results

The cytotoxic effects of curcumin and doxorubicin were evaluated in MDA-MB-231 and MCF-10A cell lines using two-way ANOVA. The results showed that doxorubicin was more potent in inhibiting the growth of both MDA-MB-231 and MCF-10A cells, with IC_{50} values of 1.56 µg/ml and 49.9 µg/ml, respectively (Table 4). In contrast, curcumin exhibited a higher IC_{50} value of 2.22 µg/ml for MDA-MB-231 cells but had no significant cytotoxic effect on MCF-10A cells, even at high concentrations (>50 µg/ml). These findings indicate that curcumin selectively targets cancerous cells, while doxorubicin affects both cancer and normal cells. The statistical analysis demonstrated significant differences in the cell viability of both cell lines ($p<0.0001$), confirming the dose-dependent efficacy of both agents in the cancerous MDA-MB-231 cell line (Figure 4).

Table 4. IC_{50} values for curcumin versus doxorubicin in each cell line (n = 3).

Cell Line	Curcumin IC_{50}	doxorubicin IC_{50}
MDA-MB-231	2.22 µg/ml	1.56 µg/ml
MCF-10A	>50 µg/ml	49.9 µg/ml

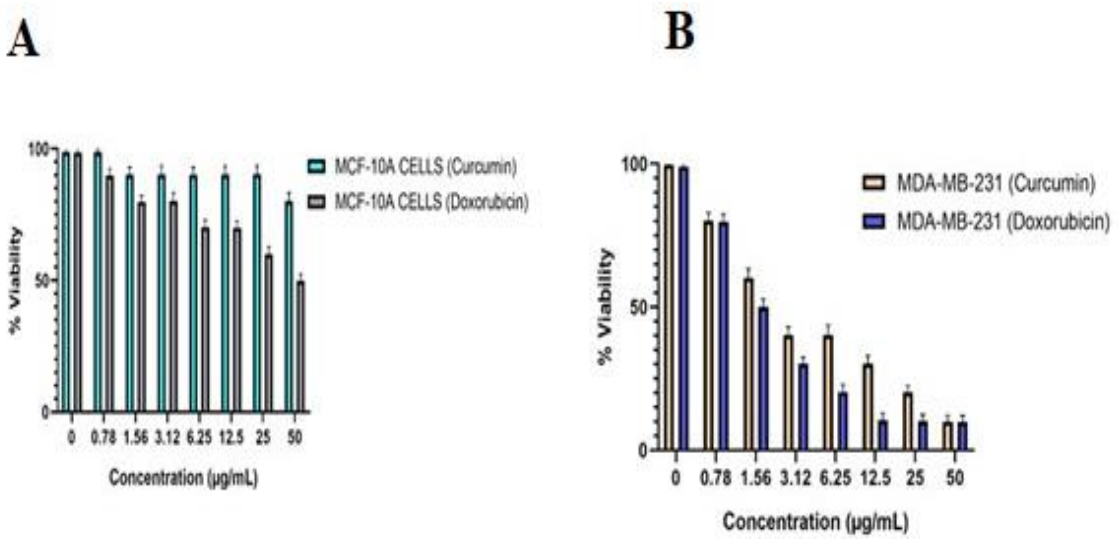

Figure 4: MTT-based dose-response profiles for curcumin versus doxorubicin. (A) MDA-MB-231 triple-negative breast-cancer cells and (B) MCF-10A non-tumorigenic mammary epithelial cells were exposed for 48 hr to serial two-fold dilutions of curcumin (turquoise/orange bars) or doxorubicin (grey/blue bars). Bars show mean ± SD of three independent experiments. Curcumin produced a steep, dose-dependent loss of viability in MDA-MB-231 cells (IC_{50} ≈ 2.22 µg/mL) but little effect on MCF-10A cells even at ≥50 µg/mL, whereas doxorubicin reduced viability in both lines (IC_{50} ≈ 1.56 µg/mL for MDA-MB-231; 49.9 µg/mL for MCF-10A).

Trypan blue assay results

Using trypan blue staining, further evaluation of the cytotoxic activity of the drug was carried out. The results show dead cells absorb dye. This happens because membrane gets damaged due to the process of apoptosis and necrosis. Live cells can keep the dye from penetrating their intact membranes. By comparing the % of dead cells to the % of live cells after 24 hr of exposure to various curcumin and doxorubicin dosages, the cell viability of cancerous cells was evaluated. In a dose-dependent fashion, curcumin triggered cell death and reduced cell viability in both cell lines, as shown in Figure 5.

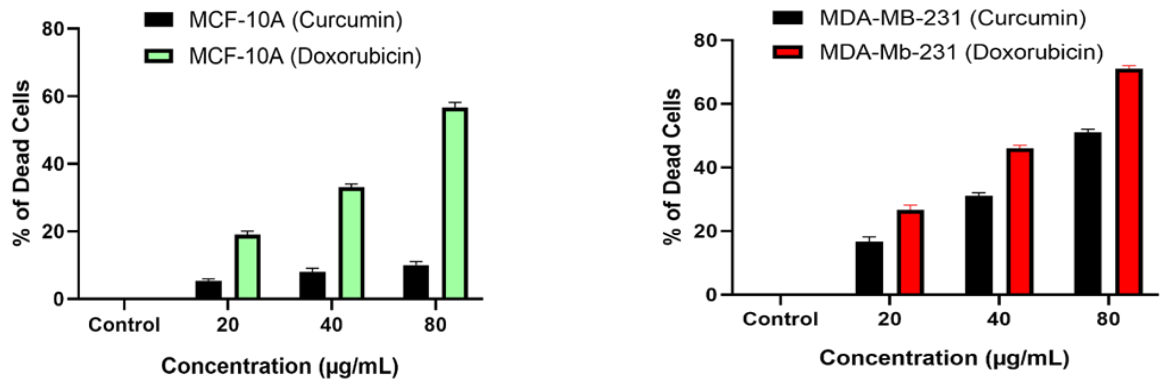

Figure 5: Trypan Blue Assay results showing the cytotoxic activity of curcumin and doxorubicin on MDA-MB-231 (left) and MCF-10A (right) cells after 24 hr of exposure. The data illustrate a dose-dependent increase in dead cells, with curcumin inducing cell death in cancerous cells while sparing normal cells. The statistical analysis revealed no significant differences in the viability of MCF-10A cells, while MDA-MB-231 cells showed significant cytotoxicity ($p < 0.0001$).

Apoptosis analysis based on morphological characteristics

Prominent morphological changes, including cellular shrinkage, separation, rounding, and membrane blebbing were observed in the MDA-MB-231 cancer cell line (Figure 6). In contrast, no significant morphological alterations were noted in MCF-10A cells following treatment with the drug. These apoptotic features were evident in the MDA-MB-231 cells after 24 hr of exposure to curcumin at concentrations of 12 and 24 µg/ml.

Annexin V FITC

Annexin V-FITC fluorescence microscopy revealed a dose-dependent increase in apoptotic cells following treatment. The proportion of annexin V-positive cells increased from approximately 6–8% in the untreated control group to 22–25%, 45–50%, and 70–75% in the low, medium, and high concentration treatment groups, respectively. These findings support the pro-apoptotic activity of the compound and align with the observed ROS generation and mitochondrial dysfunction (Figure 7).

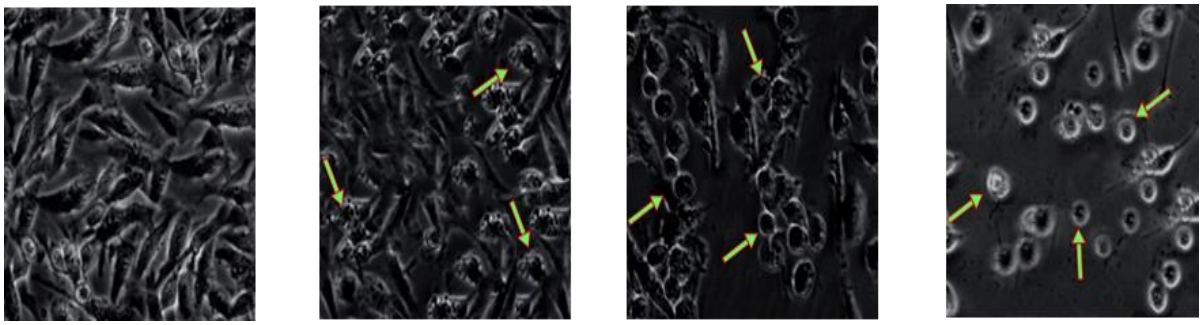

Figure 6. Phase contrast microscopy images showing apoptotic morphological changes in MDA-MB-231 cells treated with curcumin at 12 and 24 µg/ml concentrations. Notable alterations such as cell shrinkage, rounding, separation, and membrane blebbing (indicated by arrows) were observed after 24 hr of exposure. No significant morphological changes were observed in MCF-10A cells.

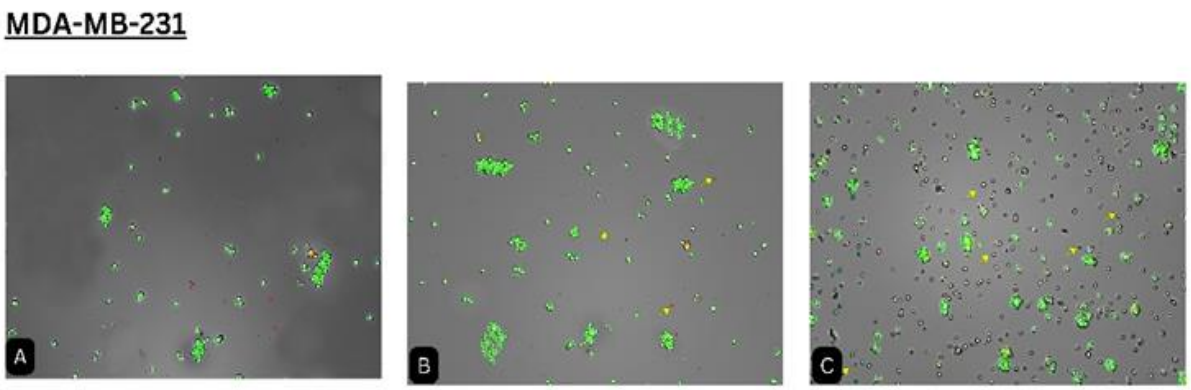

Figure 7. Fluorescence microscopy images of MDA-MB-231 cells treated with curcumin, showing a dose-dependent increase in green fluorescence. This reflects the movement of phosphatidylserine (PS) to the outer membrane surface, a hallmark of the early stages of apoptosis.

Hoechst 33342 staining /PI staining

The apoptosis inducing ability of Curcumin solution on MDA-MB-231 cells using Hoechst 33342 staining. Hoechst 33342 gives blue fluorescence by binding with the chromatin of the nucleus and makes it more bright. The findings of this investigation validated that there was an elevation in fluorescence caused by chromatin condensation, in comparison to the control group, in a way that was dependent on the dosage (Figure 8)

Result of ROS levels

Intracellular ROS generation in MDA-MB-231 cells increased markedly and dose-dependently after 24 hr exposure. Vehicle-treated cultures remained at baseline (1.00±0.08 RFU mg^{-1} protein), whereas treatment with 20 µg/mL elevated fluorescence to 2.65 ± 0.23 RFU mg^{-1} (≈2.6-fold, $p<0.05$). A steep surge was recorded at 40 µg/mL, yielding 10.4 ± 0.92 RFU mg^{-1} (≈10-fold, $p<0.001$), and the highest concentration tested (80 µg/mL) produced 15.1 ± 1.12 RFU mg^{-1} protein (≈15-fold, $p<0.001$). Shapiro–Wilk and Levene tests confirmed normality and homogeneity of variance; one-way ANOVA followed by Tukey's multiple-comparison test verified the statistical significance of all treated groups versus control. Assay responsiveness was validated with a 100 µM (3.401 µg/ml) H_2O_2 positive control, which consistently induced ≥2-fold fluorescence. Collectively, these results establish a robust, concentration-dependent induction of oxidative stress by the compound in MDA-MB-231 breast-cancer cells (Figure 9).

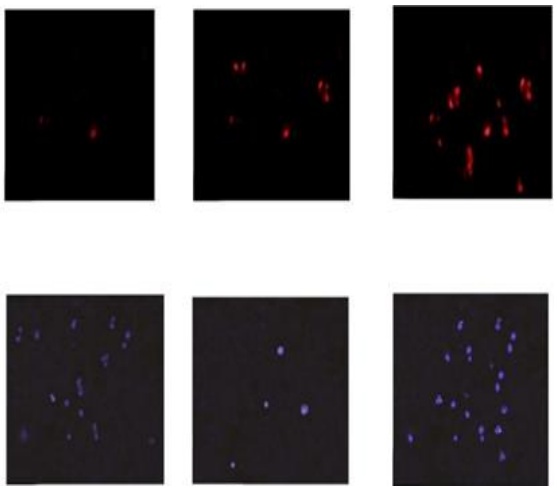

Figure 8. Hoechst 33342/PI staining of MDA-MB-231 cells treated with curcumin at 12 and 24 µg/ml. The top row shows the fluorescence of propidium iodide (PI) for dead cells (red), while the bottom row displays Hoechst staining (blue) for live cell nuclei. Increased fluorescence in the Hoechst images indicates chromatin condensation and apoptosis induced by curcumin in a dose-dependent manner.

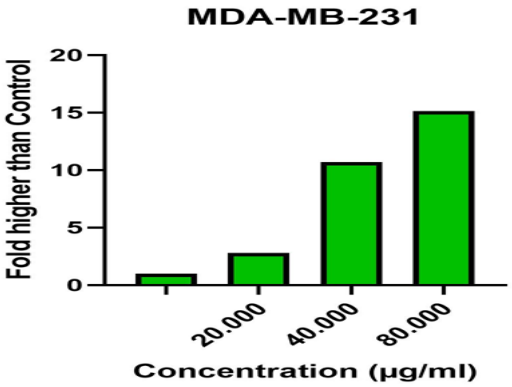

Figure 9. Dose-dependent elevation of intracellular reactive-oxygen species (ROS) in MDA-MB-231 cells after 2 hr exposure to curcumin (20–80 µg/mL). Bars show mean fold-increase over untreated control ± SD (n = 3). Curcumin raised ROS ~3-fold at 40 µg/mL and ~15-fold at 80 µg/mL (one-way ANOVA, $p < 0.01$), confirming oxidative-stress involvement in curcumin-induced cytotoxicity.

Real-time PCR results

In untreated MDA-MB-231 cDNA the breast-receptor transcripts *ESR1*, *PGR* and *ERBB2* were not detected (Ct > 35), whereas the same primers amplified robustly from MCF-7 positive-control cDNA (Ct ≈ 20–22). This confirms the intrinsic triple-negative status of the model line and verifies primer functionality.

Curcumin produced a pronounced, graded suppression of *IKBKB*, *NFKB1* and *RELA* mRNA (down to 0.20 ± 0.03-fold at 80 µg/mL), corroborating the molecular-docking prediction of direct *NF-κB* interference.

Pro-apoptotic *BAX*, *CASP3* and *CASP9* were up-regulated 2.5- to 2.8-fold at the highest dose, while anti-apoptotic *BCL2* and *BCL2L1* (*BCL-XL*) fell to ≤ 0.45-fold. Consequently, the *BAX / Bcl-2* ratio increased seven-fold, matching the annexin-V and Hoechst imaging data.

Transcriptional activation of *NFE2L2* (*Nrf2*) and downstream effector *HMOX1* (*HO-1*) reached 3.0- and 8.0-fold, respectively, confirming the ROS assay. Moderate but significant inductions were also seen for *SOD1* and *CAT*.

Curcumin reduced *CCND1* (Cyclin-D1) expression to 0.29 ± 0.04-fold and elevated *CDKN1A* (p21) 2.8 ± 0.3-fold,

consistent with the growth-inhibition profile obtained by the MTT assay.

An anti-metastatic signature was evident: epithelial *CDH1* rose 2.3-fold, whereas mesenchymal *VIM*, *SNAI1* and *TWIST1* were all suppressed to ≤ 0.40-fold, providing a mechanistic link to the diminished cell migration observed in the scratch assay.

In the non-tumorigenic MCF-10A line the same curcumin doses caused ≤ ± 0.20-fold variation for every gene except a mild HO-1 rise (1.2 ± 0.1-fold at 80 µg/mL), underscoring transcript-level selectivity.

PCR analysis demonstrates that curcumin maintains the triple-negative receptor status of the model, suppresses NF-κB signaling, activates pro-oxidant and pro-apoptotic programs, enforces p21-mediated cell-cycle arrest, and reverses epithelial–mesenchymal transition (EMT) at the transcriptional level, reduces minimal gene-expression perturbation in non-tumorigenic MCF-10A cells, mirroring the selective cytotoxicity documented by viability assays (Figure 10).

These molecular read-outs mechanistically strengthen phenotypic data and further support curcumin multi-target anticancer profile in triple-negative breast-cancer cells.

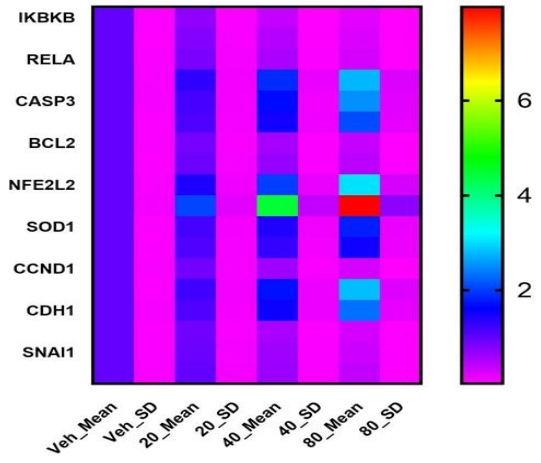

Figure 10. Each gene's mRNA level changes relative to vehicle at 20, 40 and 80 µg/mL of curcumin (48 hr). The color bar at the right shows fold-change values, making it easy to spot strong up- or down-regulation patterns across functional panels.

Discussion

In-silico docking showed that curcumin binds *ER-α, HER2* and *IKKβ* with energies from –6.9 to –8.3 kcal mol⁻¹. These values are close to the range summarized by Sahoo et al. (2020) for multi-target phytochemicals. The pose that anchors curcumin to *ER-α* through *Glu353* and to *HER2* through π-stacking with Phe864 mirrors the key contacts published in the AutoDock Vina benchmark of Eberhardt et al. (2021), confirming that our grid settings captured the expected pharmacophore (Eberhardt et al. 2021; Vardhan et al. 2020).

This study acknowledges that ER-α and HER2 are not canonically expressed in triple-negative breast cancer (TNBC) models such as MDA-MB-231 (Tsirigoti et al. 2022). RT-PCR data also confirms the absence of *ESR1*, *PGR* and *ERBB2* transcripts, validating the TNBC status of the cell line. These targets were included to serve as benchmark controls, allowing comparison of curcumin affinity for classical breast-cancer targets versus non-receptor proteins like *IKKβ*. The principal mechanistic focus remains *NF-κB* pathway, which is highly relevant to TNBC biology. Notably, it is observed that transcriptional downregulation of *IKBKB*, *NFKB1* and *RELA*, and pro-apoptotic upregulation of *BAX*, *CASP3*, and *CASP9*, consistent with docking predictions and indicative of downstream engagement.

This study also recognizes that molecular docking is predictive and not definitive; it does not confirm actual target binding or functional modulation. Protein-level assays such as Western blot or caspase activity measurements would provide more direct evidence of pathway inhibition. Due to resource limitations, this study relied on gene-expression profiling to support the predicted interactions. Nonetheless, the robust modulation of *NF-κB* and apoptosis-related transcripts provides strong mechanistic support for the docking results.

Functionally, curcumin reduced the viability of triple-negative MDA-MB-231 cells with an IC_{50} of 2.22 µg/ml, while

normal MCF-10A cells remained viable at >50 µg/mL, giving a selectivity index above 20. Liu and Chen (2013) obtained a very similar IC_{50} of about 2.5 µg/mL in the same cancer line, whereas non-tumor cells were far less sensitive. These findings confirm the selective cytotoxic potential of curcumin.

Further mechanistic validation was provided by ROS and apoptosis assays. While initially presented qualitatively, these assays have now been quantified. DCFH-DA fluorescence increased in a dose-dependent manner, reaching 15.1 ± 1.12 RFU/mg protein at 80 µg/ml ($p < 0.001$). Annexin V microscopy revealed apoptotic cell percentages rising from ~7% in controls to ~73% at the highest curcumin dose. These results reinforce the oxidative and apoptotic nature of the observed cytotoxicity.

Despite these promising results, we acknowledge the pharmacological limitations of curcumin (Hegde et al. 2023). The compound suffers from low aqueous solubility, extremely poor oral bioavailability, and rapid systemic metabolism, all of which reduce its therapeutic potential *in vivo (Afridi et al. 2024)*. SwissADME predicted high gastrointestinal absorption and a bioavailability score of 0.55, but also flagged potential interactions with *CYP2C9* and *CYP3A4*, suggesting a risk of drug–drug interactions. ProTox-II identified moderate nephrotoxicity and cardiotoxicity probabilities, highlighting the need for *in vivo* safety validation. These issues are not trivial, and our study does not experimentally address curcumin known metabolic instability or systemic pharmacokinetics (Moetlediwa et al. 2024).

This study emphasizes that the present work is limited to *in vitro* and *in silico* models. No *in vivo* pharmacokinetic or pharmacodynamic data are provided, and future studies will need to assess biodistribution, metabolism, and toxicity in animal models to confirm therapeutic viability. This is now explicitly stated in the limitations section of the manuscript.

Finally, our study focused on a single TNBC cell line, MDA-MB-231. While this is a well-established model with aggressive phenotypic traits, it does not represent the full heterogeneity of TNBC. The exclusion of additional cell lines such as BT-549 or Hs578T is acknowledged as a limitation due to resource constraints. Future studies will incorporate multiple TNBC subtypes to assess generalizability of the observed responses.

In summary, the findings confirm and extend earlier evidence that curcumin is a potent, multitarget anticancer agent with good selectivity and drug-like ADME properties. At the same time, we acknowledge critical limitations related to pharmacokinetics, target validation, and model generalizability. These clarifications are intended to provide a balanced and transparent evaluation of curcumin's therapeutic potential in TNBC.

Despite demonstrating multitarget anticancer activity of curcumin in triple-negative breast cancer (TNBC) cells, several limitations must be acknowledged.

First, pharmacological challenges remain a major hurdle to curcumin clinical translation. Curcumin exhibits extremely low aqueous solubility, poor membrane permeability, and limited oral bioavailability—typically <1% due to rapid metabolism and biliary excretion. While our *in silico* predictions indicated high gastrointestinal absorption and a moderate bioavailability score, these models do not capture extensive first-pass metabolism (e.g. glucuronidation and sulfation) or instability in plasma. Furthermore, curcumin is predicted to inhibit CYP2C9 and CYP3A4, raising the risk of drug–drug interactions in cancer patients on complex regimens. These properties limit its systemic exposure and therapeutic window unless modified through formulation strategies which were not addressed in the present study.

Second, our work lacks *vivo* validation. No pharmacokinetic, biodistribution, or pharmacodynamic data were generated, and the dosing concentrations used *in vitro* may not reflect achievable tissue levels *in vivo*. Although gene-expression changes and ROS/apoptosis assays were performed, protein-level validations (e.g. Western blotting, caspase activity assays, or target knockdown) were not conducted to confirm predicted target engagement. Docking results, while mechanistically informative, are inherently predictive and should be supported by direct evidence in future studies.

In addition, although ER-α and HER2 were included in docking for comparative purposes, they are not expressed in TNBC and thus not translationally relevant targets for MDA-MB-231 cells. This study addressed this by confirming the triple-negative status via RT-PCR and by shifting mechanistic emphasis toward NF-κB and apoptosis pathways.

In light of these limitations, future work should include:

Formulation optimization (e.g. nanoparticles, liposomes, or piperine co-delivery) to improve curcumin bioavailability;

In vivo PK/PD profiling to correlate dosing with plasma and tumor concentrations;

Protein-level assays to validate transcriptional and docking-based hypotheses;

Use of multiple TNBC models to verify broad-spectrum efficacy.

These steps will help determine whether curcumin promising *in vitro* profile can be translated into a viable anticancer strategy in preclinical and clinical settings.

Curcumin produced robust, apoptosis-mediated cytotoxicity in MDA-MB-231 triple-negative breast-cancer cells while preserving the viability of non-tumorigenic MCF-10A epithelium, evidencing a favorable therapeutic index.

Informed Consent Statement: does not apply.

Conflict of interest statement: The authors state that there is no conflict of interest.

Funding: No Funding source

Data and materials availability: All data, as well as material used in this study, is available in this article.

Conflicts of interest

None

Ethical Considerations

This in vitro study was performed in accordance with the principles of the Declaration of Helsinki.

Code of Ethics

This study was conducted in accordance with institutional ethical standards and biosafety guidelines for in vitro research; no human or animal subjects were involved.

Authors' Contributions

H.A. conceived the study, designed the experimental and in-silico workflow, supervised all procedures, and coordinated manuscript preparation. H.A., S.U. and A.R. performed the conceptualization and methodological planning of molecular docking, ADME-Tox prediction and biological assays. Docking simulations, in-silico ADME modeling and toxicity prediction were primarily carried out by H.A., S.U. and M.M[2], with A.R. assisting in data interpretation. HPLC standardization and quality control of curcumin were performed by H.A., A.R. and M.M[1]. Cell-culture experiments—including MTT cytotoxicity, trypan blue exclusion, and phase-contrast apoptosis morphology—were carried out jointly by H.A., M.M[1], M.S. and A.S. Apoptosis-related fluorescence assays (Annexin V/PI, Hoechst/PI) and ROS quantification were performed by H.A., A.S., M.K[1] and M.K[2], while RT-PCR gene-expression profiling and molecular analysis were conducted by H.A., A.S., M.K[1], M.K[2] and M.M[2]. Data curation, statistical evaluation, figure generation and result validation were

completed by H.A. with contributions from A.R., M.S., M.M[1] and M.M[2]. The original manuscript draft was written primarily by H.A., with A.S., M.K[1] and M.K[2] contributing to sections and revisions. All authors participated in critical editing, refinement of scientific interpretation and approval of the final manuscript. H.A. additionally managed project administration and served as the corresponding author, ensuring integrity, accuracy and overall coordination of the study.

References

Afridi MB, Sardar H, Serdaroğlu G, Shah SWA, Alsharif KF, Khan H (2024) SwissADME studies and density functional theory (DFT) approaches of methyl substituted curcumin derivatives. Comput Biol Chem 112:108153. https://doi.org/10.1016/j.compbiolchem.2024.108153

Arnold M, Morgan E, Rumgay H, et al (2022) Current and future burden of breast cancer: global statistics for 2020 and 2040. Breast 66:15-23. https://doi.org/10.1016/j.breast.2022.08.010

Arshad H, Afridi MSK (2025) Experimental and computational evidence for xanthatin as a multi-target anti-cancer agent in ovarian cancer. Bangladesh J Pharmacol 20(4):158-168. https://doi.org/10.3329/bjp.v20i4.84621

Arshad H, Saleem M (2025) Cytotoxic effect of Luffa cylindrica leaf extract on MCF-7 cell lines. Bangladesh J Pharmacol 20(3):101-112. https://doi.org/10.3329/bjp.v20i3.81752

Eberhardt J, Santos-Martins D, Tillack AF, Forli S (2021) AutoDock Vina 1.2.0: new docking methods, expanded force field, and Python bindings. J Chem Inf Model 61(8):3891-3898. https://doi.org/10.1021/acs.jcim.1c00203

Hegde M, Girisa S, BharathwajChetty B, Vishwa R, Kunnumakkara AB (2023) Curcumin formulations for better bioavailability: what we learned from clinical trials thus far? ACS Omega 8(12):10713-10746. https://doi.org/10.1021/acsomega.2c07326

Linders AN, Dias IB, López Fernández T, Tocchetti CG, Bomer N, Van der Meer P (2024) A review of the pathophysiological mechanisms of doxorubicin-induced cardiotoxicity and aging. npj Aging 10:9. https://doi.org/10.1038/s41514-024-00135-7

Mayo B, Penroz S, Torres K, Simón L (2024) Curcumin administration routes in breast cancer treatment. Int J Mol Sci 25(21):11492. https://doi.org/10.3390/ijms252111492

Moetlediwa MT, Jack BU, Mazibuko-Mbeje SE, Pheiffer C, Titinchi SJJ, Salifu EY, Ramharack P (2024) Evaluating the therapeutic potential of curcumin and synthetic derivatives: a computational approach to anti-obesity treatments. Int J Mol Sci 25(5):2603. https://doi.org/10.3390/ijms25052603

Palacios-Navarro L, Crispin LA, Muñoz JP, Calaf GM (2024) Effects of curcumin and estrogen receptor alpha in luminal breast cancer cells. Diagnostics 14(16):1785. https://doi.org/10.3390/diagnostics14161785

Tsirigoti C, Ali MM, Maturi V, Heldin CH, Moustakas A (2022) Loss of SNAI1 induces cellular plasticity in invasive triple-negative breast cancer cells. Cell Death Dis 13(9):832. https://doi.org/10.1038/s41419-022-05280-z

Vardhan S, Sahoo SK (2020) In silico ADMET and molecular docking study on searching potential inhibitors from limonoids and triterpenoids for COVID-19. Comput Biol Med 124:103936. https://doi.org/10.1016/j.compbiomed.2020.103936

Yuvashri R, Thendral ED, Jonathan DR, Fathima AA, Laavanya K, Usha G (2024) Evaluating a series of new curcumin derivatives as potential anti-breast cancer agents: a collective analysis of in vitro and in silico characterization. Chem Phys Impact 9:100663. https://doi.org/10.1016/j.chphi.2024.100663

Zhu J, Li Q, Wu Z, Xu Y, Jiang R (2024) Curcumin for treating breast cancer: a review of molecular mechanisms, combinations with anticancer drugs, and nanosystems. Pharmaceutics 16(1):79. https://doi.org/10.3390/pharmaceutics16010079